arXiv:astro-ph/9909237v1 14 Sep 1999

EVOLUTION OF ROTATING SUPERMASSIVE STARS TO THE ONSET OF COLLAPSE

Thomas W. Baumgarte and Stuart L. Shapiro[1]

Department of Physics, University of Illinois at Urbana-Champaign, Urbana, Il 61801

Draft version February 1, 2008

ABSTRACT

We launch a fully relativistic study of the formation of supermassive black holes via the collapse of supermassive stars. Here we initiate our investigation by analyzing the secular evolution of supermassive stars up to the onset of dynamical instability and collapse. We focus on the effects of rotation, assumed uniform, and general relativity. We identify the critical configuration at which radial instability sets in and determine its structure in detail. We show that the key nondimensional ratios R/M, $T/|W|$ and J/M^2 (T is the rotational kinetic energy and W is the gravitational potential energy) for this critical configuration are universal numbers, independent of the mass, spin, radius or history of the star. We compare results from an approximate, analytic treatment with a fully relativistic, numerical calculation and find good agreement. We solve analytically for the time evolution of these parameters up to the onset of instability. Cooling by photon radiation drives the evolution, which is accompanied by mass, angular momentum and entropy loss. The critical configuration serves as initial data for a future relativistic, hydrodynamical, 3D simulation of the collapse of an unstable supermassive star. Since this implosion starts from a universal critical configuration, the collapse is also uniquely determined and should produce a universal gravitational waveform. In this paper we briefly speculate on the possible outcome of this collapse and asses to what extent it offers a promising route to forming a supermassive black hole.

1. INTRODUCTION

Recent observations provide increasingly strong evidence that supermassive black holes (SMBHs) exist and that they are the sources that power active galactic nuclei (AGNs) and quasars (see, e.g., Rees 1998, for a summary and references). For example, the 1.3 cm maser-emission line of H_2O allows for an extremely accurate mapping of gas motions in a disk at the core of the galaxy NGC 4258. The inner edge of the disk has a radius of ~ 0.1 pc, and the inferred velocity profile is consistent with Keplerian motion around a central object of $3.6 \times 10^7 M_\odot$ (Claussen & Lo 1986; Watson & Wallin 1994; Miyoshi et. al. 1995). The most conservative candidate for so massive an object in so small a volume is a black hole.

However, the scenario by which SMBHs form with masses in the range of 10^6–$10^{10} M_\odot$ is still uncertain (see Rees 1984 for an overview). Viable stellar dynamical and a hydrodynamical routes leading to the formation of SMBHs have both been proposed. In one stellar dynamical scenario, the primordial gas first fragments into stars, which form a dense stellar cluster or galaxy core. Repeated collisions and mergers of the stars in the cluster lead to the build-up of massive stars, and the subsequent collapse of the massive stars result in the formation of stellar-mass black holes. As these holes continue to swallow stars and grow, they settle toward the galaxy center, merge and trigger the build-up of one or more SMBHs (see, e.g., Quinlan & Shapiro 1990 and references therein). In another dynamical scenario, the gravothermal catastrophe (secular core collapse) in a dense cluster composed of neutron stars or stellar-mass black holes may drive the cluster core to a relativistic state. Sufficiently relativistic clusters are dynamically unstable to catastrophic collapse and may give

birth to SMBHs (Zel'dovich & Podurets 1965; Shapiro & Teukolsky 1985a, 1985b; Quinlan & Shapiro 1987). It may be more likely that the contracting primordial gas builds up sufficient radiation pressure to inhibit further fragmentation and hence prevent the formation of a stellar cluster. Alternatively, a supermassive gas cloud may build up from the fragmentation of stars in collisions in stellar clusters (Sanders 1970; Begelman & Rees 1978). In such hydrodynamical scenarios, a massive black hole may form directly from gas, perhaps after a phase in which the gas evolves in a quasistationary manner as a supermassive star (SMS). Such a phase can only be transient, since ultimately general relativity will drive such stars dynamically unstable (Iben 1963; Chandrasekhar 1964a, b; Feynman, unpublished, as quoted in Fowler 1964). The structure and evolution of supermassive stars up to the onset of instability has been explored previously by many authors, including Hoyle & Fowler (1963a, b), Fowler (1964, 1966), Bisnovatyi-Kogan, Zel'dovich & Novikov (1967), Appenzeller & Fricke (1972) and Fuller, Woosley and Weaver (1986) (see Zel'dovich & Novikov, 1971, and Shapiro and Teukolsky, 1983, for reviews and further references).

In addition to their importance for a fundamental understanding of AGNs and quasars, supermassive objects and the formation of SMBHs have recently attracted new interest because they are likely candidates for detection by currently proposed space-based gravitational wave detectors like the Laser Interferometer Space Antenna (LISA). Because of its long arm length, this detector would be very sensitive to long wavelength and low frequency radiation, and therefore supermassive objects are among the most promising sources (see, e.g., Thorne & Braginsky 1976; Thorne 1995). In particular, LISA may be able to detect

[1]Department of Astronomy and National Center for Supercomputing Applications, University of Illinois at Urbana-Champaign, Urbana, Il 61801

the collapse of a SMS to a SMBH. Even more promising is the possible detection of the coalescence of two SMBHs (LISA Pre-Phase A report 1995). The likelihood of such an event, however, largely depends on how SMBHs form and is therefore still uncertain.

In a series of papers we revisit the formation of SMBHs via the collapse of SMSs, focussing on the influence of rotation and general relativity. We analyze the secular contraction of a uniformly rotating equilibrium configuration via thermal emission and mass loss. We concentrate on a configuration rotating at the mass-shedding limit. In Baumgarte & Shapiro (1999, hereafter Paper I), we have shown that the luminosity from such a star is considerably reduced below the value of a nonrotating spherical star of the same mass.

In this paper, we analyze the structure and stability against collapse of fully relativistic, rotating $n = 3$ polytropes in stationary equilibrium. SMSs to which these calculations apply are radiation-dominated, isentropic configurations of sufficient mass that neither nuclear burning nor electron-positron pairs are important before the stars reaches the onset of relativistic gravitational instability. Stars with $M \gtrsim 10^6 M_\odot$ fall in this category (Zel'dovich & Novikov 1971; Fuller, Woosley & Weaver 1986). Moreover, the evolutionary timescale due to cooling has to be longer than the hydrodynamic timescale for the star to evolve in a quasistationary fashion. According to equations (9) and (10) below, we find that this constraint is satisfied for all masses $M \lesssim 10^{13} M_\odot$.

We track the quasistationary evolution of such stars to the point of onset of radial instability. We first identify this critical configuration analytically by means of a post-Newtonian energy variational method. As pointed out by Bisnovatyi-Kogan, Zel'dovich & Novikov (1967), determining the onset of relativistic collapse in a rapidly rotating SMS requires a *second-order* post-Newtonian analysis, not a first-order, as in the case of a nonrotating star. We provide an approximate, post-Newtonian analytic analysis (rigorizing and completing the qualitative argument of Bisnovatyi-Kogan, Zel'dovich & Novikov (1967) and Zel'dovich & Novikov (1971), who only provide a dimensional estimate of the second post-Newtonian term). Then, to establish the result rigorously, we use a recent numerical code (Cook, Shapiro & Teukolsky 1992, 1994) to construct rotating equilibrium models in full general relativity. We show that the mass of the critical configuration is a unique function of the specific entropy. The values of R/M, $T/|W|$ and J/M^2 at the onset of collapse are universal numbers, independent of the mass or prior evolution. Here M is the mass, R the (polar) radius, J the angular momentum, T the rotational and W the gravitational potential energy of the star. We also speculate on the likely outcome of collapse for stars which do not disrupt due to thermonuclear explosions during collapse; it is found that stars with $M > 10^5 M_\odot$ and initial metallicities $Z < 0.005$ do not explode (Fuller, Woosley & Weaver 1986). Since these stars start collapsing from a universal critical configuration, the subsequent collapse is also uniquely determined and should produce a unique gravitational waveform. We postpone a detailed discussion of this phase for a future paper in which we follow the dynamical collapse numerically in general relativity (Baumgarte,

Shapiro & Shibata 1999).

The key goals of our study are to decide whether a SMBH can really emerge from the collapse of a SMS and to determine the hole parameters if indeed it can be formed this way. Alternatively, a rotating supermassive cloud or star could collapse to a weakly relativistic disk (e.g. Wagoner 1969; Loeb & Rasio 1994). If the collapsing innermost region enters the strong-field domain, the angular momentum of this matter must be below the maximum value of a Kerr hole ($J/M^2 = 1$) for black hole formation to occur eventually. What happens if the angular momentum exceeds this limit? Does angular momentum dissipation by outflowing gas allow for black hole formation of the core? Or, does gravitational radiation, following the formation of bars or axial currents carry away enough angular momentum to permit collapse? Finally, if a SMBH can form by the collapse of a SMS, what is its mass and spin given the mass and spin of the SMS at the onset of collapse?

In this paper we deal primarily with the structure, stability and early secular evolution phases of the SMS scenario. Our calculation, in effect, sets up the initial data at the onset of collapse. Tracking the subsequent dynamical evolution of these initial data will resolve the key questions posed above, and in this paper we will only speculate briefly on the outcome of the dynamical collapse.

This paper is organized as follows: In Section 2 we provide a qualitative overview of the problem and present our basic assumptions. In Section 3 we discuss the equilibrium and stability of rotating, relativistic SMSs. In particular, we determine the critical configuration at which an evolving SMS becomes dynamically unstable to radial perturbations. We compare results from an approximate analytical treatment (Section 3.2) with those from a numerical, fully relativistic calculation (Section 3.3). Having identified the onset of instability, we then solve analytically for the evolution of SMSs during the secular contraction phase up to this critical configuration in Section 4. In Section 5 we provide some qualitative arguments which suggest that the direct formation of SMBHs from the collapse of SMSs indeed may be possible. We summarize and discuss our results in Section 6. Except where noted otherwise, we adopt geometrized units with $c \equiv 1 \equiv G$ throughout this paper.

2. QUALITATIVE OVERVIEW AND BASIC ASSUMPTIONS

SMSs may form if collapsing primordial gas builds up enough entropy so that the radiation pressure can slow down the collapse (see Begelman & Rees, 1978, for an alternative scenario). Further contraction will then spin up the newly formed SMS to the mass-shedding limit, provided that the gas had some initial angular momentum and that viscosity maintains uniform rotation. The SMS will then evolve secularly along the mass-shedding limit, simultaneously emitting radiation, matter and angular momentum (see, e.g., Bisnovatyi-Kogan, Zel'dovich & Novikov 1967; Zel'dovich & Novikov 1971). Once it reaches the onset of radial instability, the star collapses on a dynamical timescale, and may ultimately form a SMBH.

For sufficiently massive objects ($M \gtrsim 10^6 M_\odot$), the equation of state is dominated by thermal radiation pressure. It can also be shown that SMSs are convective (see Loeb & Rasio 1994, for a simple proof) with constant en-

tropy per baryon,

$$s \approx \frac{4}{3} \frac{aT^4}{n_b},$$ (1)

where n_b is the baryon density and a is the radiation density constant. These conditions imply that the structure of a SMS is that of an $n = 3$ polytrope

$$P = K\rho^{4/3},$$ (2)

where

$$K = K(s) = \frac{a}{3} \left(\frac{3s}{4m_H a}\right)^{4/3} = const.$$ (3)

(see eq. 17.2.6 in Shapiro & Teukolsky 1983). Here, m_H is the mass of a hydrogen atom and K has been evaluated for a composition of pure ionized hydrogen. In Newtonian theory, the mass of a static, equilibrium $n = 3$ polytrope is *uniquely* determined by the polytropic constant K alone

$$M = \left(K \frac{k_1}{k_2}\right)^{3/2}$$ (4)

(the numerical coefficients k_1 and k_2, derived from Lane-Emden functions, are given in Table 1 below). Inverting this relation, we can write K in terms of M as

$$K = 1.01 \times 10^3 \, \text{cm}^{2/3} \left(\frac{M}{M_\odot}\right)^{2/3},$$ (5)

Since $n = 3$ polytropes are extremely centrally condensed, the self-gravity of the outermost envelope of a uniformly rotating configuration can be neglected and the Roche approximation (see Section 3.1) can be applied.

In Newtonian gravitation, $n = 3$ polytropes are marginally stable to radial collapse. However, even very small general relativistic corrections make these polytropes unstable, and some mechanism has to be invoked to prevent collapse. In this paper, we focus on rotation, which up to a critical configuration along the mass-shedding sequence can stabilize SMSs. In Section 3 we will identify this critical configuration (which we will call "configuration A"). Alternatively, gas pressure may stabilize SMSs in the absence of angular momentum (see Zel'dovich & Novikov 1971; Shapiro & Teukolsky 1983), but even a small degree of rotation will dominate gas pressure (cf. Section 3.2). A dark matter background also tends to have a stabilizing effect (Fuller, Woosley & Weaver, 1986), but it is also much less important than rotation (Bisnovatyi-Kogan 1998). Since the ratio between the rotational kinetic and the potential energy, $T/|W|$, is always very small for a uniformly rotating star during secular evolution along the mass-shedding sequence (see eq. [19] and Figure 4), it is unlikely that nonradial modes of instability are important during this phase. Once the star has become unstable and collapses, however, $T/|W|$ can become very large, and it is likely that such nonradial modes develop (see Section 5).

Massive enough stars ($M \gtrsim 10^6 M_\odot$) do not reach sufficiently high temperatures for nuclear burning to become important before reaching the onset of instability (see Section 3.4). Also, electron-positron pairs play a negligible role in this regime (Zel'dovich & Novikov 1971). The evolution of the SMS along the mass-shedding sequence is then determined solely by cooling via thermal photon emission and loss of mass and angular momentum. As we have shown in Paper I, the luminosity of a rotating supermassive star at mass-shedding is

$$L = 0.639 \, L_{\text{Edd}},$$ (6)

where the Eddington luminosity is

$$L_{\text{Edd}} = \frac{4\pi M}{\kappa}.$$ (7)

The opacity κ is dominated by Thomson scattering off free electrons

$$\kappa = \kappa_T = 0.2 \, (1 + X_H) \, \text{cm}^2 \text{g}^{-1},$$ (8)

where X_H is the hydrogen mass fraction. For $M \gtrsim 10^5 M_\odot$, temperatures are low enough that Klein-Nishina corrections can be neglected (see, e.g., Fuller, Woosley & Weaver 1986).

As we will find in Section 4, the evolutionary timescale for secular evolution along the mass-shedding sequence is given by

$$t_{\text{evol}} = 8.8 \times 10^{11} \text{s} \left(\frac{R/M}{456}\right)^{-1}$$ (9)

where the coefficient has been evaluated near the critical configuration (see eq. (67)). The dynamical timescale is

$$t_{\text{dyn}} \sim (G\rho_c)^{-1/2}$$ (10)
$$= 1.3 \times 10^{-2} \text{s} \left(\frac{M}{M_\odot}\right) \left(\frac{\bar{\rho}_c}{7 \times 10^{-9}}\right)^{-1/2},$$

where we have used eq. (39) below to evaluate ρ_c in terms of the non-dimensional density $\bar{\rho}_c$. Given the critical values for $\bar{\rho}_c$ and R/M that we find in Section 3, the evolutionary timescale is longer than the dynamical timescale for $M \lesssim 6.7 \times 10^{13} M_\odot$. This mass is larger than the value derived in Shapiro & Teukolsky (1983), where a similar estimate has been made for nonrotating SMSs stabilized by gas pressure.

Also important is the viscous timescale, which is very uncertain. Not surprisingly, the microscopic viscosity due either to collisions between ions or to radiation yields timescales which are larger than the evolutionary timescale by many orders of magnitude (see Kippenhahn & Weigert 1990). The effect of turbulent viscosity can be estimated by assuming that the velocity of the turbulent motion v_t is an appreciable fraction of the velocity of sound,

$$v_t = \alpha v_{\text{sound}},$$ (11)

where we take the dimensionless viscosity parameter α to lie in the range

$$0.01 \lesssim \alpha \lesssim 1$$ (12)

(see Shakura & Sunyaev 1973; also Zel'dovich & Novikov 1971; Balbus & Hawley 1991). Assuming the characteristic scale of nonuniformity to be some fraction of the stellar radius R, we can then estimate the turbulent viscosity to be

$$\eta_t \sim \rho R v_t = \rho R \alpha v_{\text{sound}}.$$ (13)

The corresponding timescale is then

$$t_{\rm vis} \sim \frac{R^2\rho}{\eta_t} \sim \frac{R}{\alpha v_{\rm sound}} \sim \alpha^{-1} t_{\rm dyn}. \qquad (14)$$

It has been argued that both convection and magnetic fields serve to generate such a turbulent viscosity in SMSs (Bisnovatyi-Kogan, Zel'dovich & Novikov 1967; Wagoner 1969).

For SMSs with masses $M \ll 6.7 \times 10^{11} M_\odot$, we therefore find the hierarchy

$$t_{\rm dyn} \ll t_{\rm vis} \ll t_{\rm evol}. \qquad (15)$$

Eq. (15) justifies our assumption that the star evolves in a quasistationary manner along the mass-shedding sequence. The last inequality implies that turbulent viscosity, if present, will keep the SMS in uniform rotation. We will assume this result in treating the secular evolution up to the onset of instability. Once the star becomes unstable and starts collapsing, however, the evolution will proceed on the dynamical timescale, and it is unlikely that the viscosity will be efficient enough to maintain uniform rotation. It is more likely that cylindrical mass shells will conserve their angular momentum, which we assume for our qualitative arguments in Section 5.

3. EQUILIBRIUM AND STABILITY

In this Section we analyze the equilibrium and stability of rotating SMSs and identify the critical configuration at which radial instability sets in. We briefly review the predictions of the Roche approximation in Section 3.1. In Section 3.2 we present an analytic, post-Newtonian model calculation, which provides qualitative insight into the scaling behavior and approximate numerical parameters for the critical configuration. In Section 3.3, we present numerical results from a fully relativistic calculation, which allows us to identify the critical configuration and its characteristic parameters (including J/M^2 and R/M) independently of the approximations used in the analytical treatment (including the post-Newtonian and Roche approximation). We find remarkable agreement between the two calculations. Lastly, in Section 3.4, we restore cgs units and provide expressions for the physical parameters in SMSs.

3.1. *Predictions of the Roche Model*

The Roche approximation for rotating $n = 3$ polytropes has been derived and discussed in the literature (see, e.g., Zel'dovich & Novikov 1971; Shapiro & Teukolsky 1983). Here we briefly summarize the key elements for application below (see also Paper I).

Stars with soft equations of state are extremely centrally condensed: they have an extended, low density envelope, with the bulk of the mass concentrated in the core. For an $n = 3$ polytrope, for example, the ratio between central density to average density is $\rho_c/\langle\rho\rangle = 54.2$. The gravitational forces in the envelope are therefore dominated by the massive core, and it is appropriate to neglect the self-gravity of the envelope. In this case, it is easy to show that matter at the equator of a rotating star orbits with the Kepler frequency when the ratio between the equatorial radius R_e and the polar radius R_p reaches

$$\left(\frac{R_e}{R_p}\right)_{\rm shedd} = \frac{3}{2}. \qquad (16)$$

At this point, the angular velocity of the star assumes its maximum value before mass-shedding from the equator sets in:

$$\Omega_{\rm shedd} = \left(\frac{2}{3}\right)^{3/2} \left(\frac{M}{R_p^3}\right)^{1/2}. \qquad (17)$$

The polar radius hardly changes from the value of the radius of the nonrotating, spherical star, a result which has been verified numerically (Papaloizou & Whelan 1973). Since the bulk of the matter is concentrated at the core and hardly affected by the rotation, the moment of inertia of inertia of the star barely changes with rotation and is well approximated by the nonrotating value

$$I = \frac{2}{3}\langle r^2\rangle M = \frac{2}{3} 0.1130\, R_p^2 M, \qquad (18)$$

where the brackets denote a mass weighted average over the star, and where the last equality holds for $n = 3$ (this approximation turns out to be less accurate; cf. Section 3.3). The ratio between the kinetic and potential energy at mass-shedding then becomes

$$\begin{aligned}\left(\frac{T}{|W|}\right)_{\rm shedd} &= \frac{(1/2)I\,\Omega_{\rm shedd}^2}{(3/2)M^2/R_p}\\ &= \left(\frac{2}{3}\right)^4 \frac{0.1130}{3} = 0.00744. \end{aligned} \qquad (19)$$

This result predicts that $T/|W|$ of a maximally rotating, $n = 3$ polytrope (or any star for which the Roche approximation applies) is a universal constant, independent of mass, radius, or orbital velocity. In Section 3.3 we will see that precise numerical models predict a somewhat larger value of $T/|W|$, which nevertheless also remains approximately constant along a mass-shedding trajectory (see Figure 4 below).

3.2. *Analytical Model*

To determine the equilibrium and stability of a rotating SMS, we write its total energy as the sum of the internal energy U, the potential energy W, the rotational energy T, a post-Newtonian correction E_{PN} and a post-post-Newtonian correction E_{PPN}. For a $n = 3$ polytrope, these terms can be written

$$E = k_1 K M \rho_c^{1/3} - k_2 M^{5/3}\rho_c^{1/3} + \qquad (20)$$
$$k_3 j^2 M^{7/3}\rho_c^{2/3} - k_4 M^{7/3}\rho_c^{2/3} - k_5 M^3\rho_c,$$

where we have defined $j \equiv J/M^2$ and have neglected corrections due to deviations from sphericity. This neglect is justified, since these corrections scale with $T/|W|$, which according to (19) is always very small. Even though the value of the post-post-Newtonian correction E_{PPN} is very small, this term is crucial for determining the critical, marginally stable configuration, as emphasized by Zel'dovich and Novikov (1971). The values of the nondimensional coefficients k_i are listed in Table 1; they are constructed from Lane-Emden functions.

Note that for any polytrope $K^{n/2}$ has units of length. We can therefore introduce nondimensional coordinates by

TABLE 1

VALUES OF THE STRUCTURE COEFFICIENTS FOR $n = 3$.

k_1	k_2	k_3	k_4	k_5
1.7558^1	0.63899^1	1.2041^1	0.918294^2	0.331211^3

REFERENCES.—(1) Lai, Rasio & Shapiro, 1993; (2) Shapiro & Teukolsky, 1983; (3) Lombardi, 1997

setting $K = 1$ (see also Cook, Shapiro & Teukolsky 1992). We will denote values of nondimensional variables in these coordinates with a bar (for example $\bar{M}$). Values of these quantities for any other value of K can be recovered easily by rescaling with an appropriate power of $K^{n/2} = K^{3/2}$; for example $M = K^{3/2}\bar{M}$ and $\rho = K^{-3}\bar{\rho}$.

Taking the first derivative of (20) with respect to the central density yields a condition for equilibrium

$$0 = \frac{\partial \bar{E}}{\partial x} = k_1 \bar{M} - k_2 \bar{M}^{5/3} + 2k_3 j^2 \bar{M}^{7/3} x -$$
$$2k_4 \bar{M}^{7/3} x - 3k_5 \bar{M}^3 x^2, \qquad (21)$$

where $x = \bar{\rho}_c^{1/3}$. For stable equilibrium, the second derivative of eq. (20) has to be positive. A root of the second derivative therefore marks the onset of radial instability

$$0 = \frac{\partial^2 \bar{E}}{\partial x^2} = 2k_3 j^2 \bar{M}^{7/3} - 2k_4 \bar{M}^{7/3} - 6k_5 \bar{M}^3 x. \qquad (22)$$

Solving eq. (22) for x immediately yields

$$\bar{\rho}_c^{1/3} = x = \frac{k_3 j^2 - k_4}{3k_5 \bar{M}^{2/3}}. \qquad (23)$$

For stability, we obviously require $\bar{\rho}_c \geq 0$ or

$$j \geq j_{\min} = \left(\frac{k_4}{k_3}\right)^{1/2} = 0.8733. \qquad (24)$$

Note that stable configurations with $j = j_{\min}$ have $\bar{\rho}_c = 0$.

SMSs with angular momenta less than $j_{\min}$ can also be stabilized by the nonvanishing contribution of the plasma, which effectively decreases the polytropic index n to a value slightly smaller than 3 (see Shapiro & Teukolsky 1983, Chapt. 17). Here, because we are interested in the effects of rotation, we neglect the plasma and approximate supermassive stars as strict $n = 3$ radiation dominated polytropes. Our neglect of gas pressure breaks down for angular momenta less than $j_{\min}$, since it would make wrong predictions for the stability of supermassive stars. We expect that most equilibria which form in nature have $j \gg j_{\min}$.

Inserting (23) into (21), we find the mass of equilibrium stars at the onset of instability is

$$\bar{M}^{2/3} = k_1 \left[k_2 - \frac{1}{3k_5} \left(k_3 j^2 - k_4\right)^2 \right]^{-1}. \qquad (25)$$

For $j = j_{\min}$, and hence $\bar{\rho}_c = 0$, the configuration has infinite radius and we obviously recover the (unique) Newtonian mass of a $n = 3$ polytrope

$$\bar{M}_{\min} = \left(\frac{k_1}{k_2}\right)^{3/2} = 4.5548 \qquad (26)$$

(where we keep enough digits for purposes of comparison later on). This configuration corresponds to point B in Figs. 2 and 3. Note that from equation (25), all critical configurations at the onset of instability have a mass greater or equal to $\bar{M}_{\min}$.

The maximum angular velocity of a rotating star occurs at mass-shedding, where we know the value of $T/|W|$ (eq. 19 in the Roche approximation). It is convenient to express $T/|W|$ in terms of x, $\bar{M}$ and j

$$\frac{T}{|W|} = \frac{k_3 j^2 \bar{M}^{7/3} x^2}{k_2 \bar{M}^{5/3} x} = \frac{k_3 j^2 \bar{M}^{2/3} x}{k_2}. \qquad (27)$$

The last stable configuration for a given $T/|W|$ can now be found by substituting (23) into (27), which yields a quadratic equation for j^2:

$$j^4 - \frac{k_4}{k_3} j^2 - 3\frac{k_2 k_5}{k_3^2} \frac{T}{|W|} = 0, \qquad (28)$$

or

$$j^2 = \frac{k_4}{2k_3} + \sqrt{\frac{k_4^2}{4k_3^2} + 3\frac{k_2 k_5}{k_3^2} \frac{T}{|W|}}. \qquad (29)$$

(The second solution can be disregarded, since it gives a negative value for j^2). To first order in $T/|W|$, this result can be approximated by

$$j = j_{\min}(1 + \frac{3}{2}\frac{k_2 k_5}{k_4^2} \frac{T}{|W|}) = j_{\min}(1 + 0.377 \frac{T}{|W|}). \qquad (30)$$

The mass of this critical configuration now can be found by inserting (30) into (25), which yields

$$\bar{M}^{2/3} = \frac{k_1}{k_2} \left(1 - 3\frac{k_5 k_2}{k_4^2}\left(\frac{T}{|W|}\right)^2\right)^{-1}, \qquad (31)$$

or, to first order in $(T/|W|)^2$,

$$\bar{M} = \bar{M}_{\min}\left(1 + \frac{9}{2}\frac{k_5 k_2}{k_4^2}\left(\frac{T}{|W|}\right)^2\right)$$

$$= \bar{M}_{\min}\left(1 + 1.1294\left(\frac{T}{|W|}\right)^2\right). \qquad (32)$$

Adopting the Roche prediction (19) for $T/|W|$, we find

$$j_{\mathrm{crit}} = 0.8757 \qquad (33)$$
$$\bar{M}_{\mathrm{crit}} = 4.5551. \qquad (34)$$

Inserting these values into (23) yields

$$(\bar{\rho}_c)_{\mathrm{crit}} = 6.6 \times 10^{-9}. \qquad (35)$$

These values correspond to the critical configuration A in Figs. 2 and 3.

It is obvious from expressions (30) and (32) that the critical values j_{crit} and $\bar{M}_{\mathrm{crit}}$ depend on several approximations. In this section, we have adopted the Roche prediction (19) for $T/|W|$ at mass-shedding, even though self-consistent numerical calculations yield a value that differs by about 20% (cf. Section 3.3 and Table 2). Moreover, the critical values depend on the second post-Newtonian coefficient k_5. We have adopted a value that only takes into account second post-Newtonian corrections to the energy of a spherical, nonrotating configuration (Lombardi 1997), and have neglected first post-Newtonian corrections to the Newtonian rotational kinetic energy. The later would have the same form as the second post-Newtonian term E_{PPN}, and would therefore introduce an unknown correction to the coefficient k_5 (which we expect to be small for small values of $T/|W|$). Together, this means that our analytic calculation can only yield approximate values for the critical configuration.

It is interesting to note, however, that our analytic model predicts j_{crit} to be less than unity, which is the maximum value allowed for a Kerr black hole. A supermassive star that evolves along the mass-shedding sequence and ultimately becomes unstable could therefore collapse to a black hole without having to loose additional angular momentum (see also Section 5).

Lastly, we estimate the compaction of the critical configuration by rewriting equation (27) in terms of the polar radius $\bar{R}_p$. Neglecting deviations from sphericity, we find

$$\frac{T}{|W|} = \frac{2\bar{J}^2\bar{R}_p}{6\bar{I}\bar{M}^2} = \frac{1}{2 \times 0.1130}\frac{\bar{M}}{\bar{R}_p}j^2 \qquad (36)$$

or

$$\frac{R_p}{M} = 4.425\frac{j^2}{T/|W|}, \qquad (37)$$

where we have dropped the bars on the left hand side, since R_p/M is a dimensionless combination, and have used eq. (18) to evaluate I. Inserting (19) and (33), we find

$$\left(\frac{R_p}{M}\right)_{\mathrm{crit}} = 456. \qquad (38)$$

This shows that the critical configuration is only very mildly relativistic, and that a post-Newtonian approximation is adequate for determining its equilibrium structure.

The small admixture of thermal gas pressure can stabilize a nonrotating SMS for values of R/M exceeding $(R/M)^{\mathrm{gas}} = 1.59\,(M/M_\odot)^{1/2}$ (eq. (17.4.11) in Shapiro & Teukolsky, 1983). For masses $M \gtrsim 10^5 M_\odot$, this ratio is larger than that given eq. (38). Consequently, rotation serves to stabilize these masses beyond the point up to which thermal pressure alone can stabilize them. Hence thermal gas pressure can be ignored, as we have done, in determining the point of onset of instability in mass-shedding configurations with $M \gtrsim 10^5 M_\odot$.

Note that all the nondimensional parameters of the critical configuration, including $T/|W|$, R/M and J/M^2, are universal constants, and do not depend on the mass of the SMS or its history.

3.3. *Numerical Results*

In this Section we present numerical models of fully relativistic, uniformly rotating $n = 3$ polytropes. We have constructed these models with the numerical code of Cook, Shapiro & Teukolsky (1992, 1994). As a typical result, we show density contours of the last stable (critical) configuration (configuration A) in a plane containing the axis of rotation in Figure 1.

In the static limit, we recover the Tolman-Oppenheimer-Volkoff result for relativistic hydrostatic equilibrium in spherical symmetry. We mark this curve by the long dashed line in Figures 2 and 3. Note that for a polytropic index $n = 3$, Newtonian gravity predicts a unique value for the mass $\bar{M}$, which is independent of the central density (equation (26)). In general relativity, $\bar{M}$ is no longer independent of $\bar{\rho}_c$, but obviously we recover the the Newtonian value in the Newtonian limit ($\bar{\rho}_c \to 0$, point B in Figures 2 and 3). Note that in general relativity all static $n = 3$ polytropes are unstable to radial perturbations ($\partial\bar{M}/\partial\bar{\rho}_c < 0$).

For each central density $\bar{\rho}_c$, there is a unique (maximum) angular momentum, at which the equator reaches the Kepler frequency, and at which mass-shedding sets in. We mark this mass-shedding curve by the short dashed line in Figures 2 and 3.

In order to find a transition from stable equilibrium to unstable equilibrium, we need to construct sequences of constant angular momentum and locate their turning points (Friedman, Ipser & Sorkin, 1988). We have marked sequences of constant angular momentum with thin, solid lines in Figures 2 and 3. They all connect the mass-shedding sequence with point B. The later can be understood by observing that, from equation (36), $T/|W|$ scales with $\bar{R}^{-1}$ for constant j. As $\bar{\rho}_c \to 0$, the mass $\bar{M}$ remains finite, and hence $\bar{R} \to \infty$. We therefore have $T/|W| \to 0$, so that rotation plays an increasingly negligible role and we recover, for any j, the static limit.

The sequences of constant angular momentum have a turning point only for a small range of angular momenta ($18.25 \lesssim \bar{J} \lesssim 20$). Above these values, the sequences are monotonically increasing, while below they are monotonically decreasing. The thick solid line in Figures 2 and 3 connects the turning points, and therefore separates a region of stable equilibrium (above the line), from a region of unstable equilibrium (below the line).

As it cools, a supermassive star evolves toward higher density along the mass-shedding sequence and is therefore

	$\bar{\rho}_c$	$\bar{M}$	R_p/M	J/M^2	$T/|W|$	R_p/R_e	$\Omega/\Omega_{\mathrm{spher}}$[a]	I/I_{spher}[b]
Analytical Model	6.6×10^{-9}	4.5551	456	0.8757	7.44×10^{-3}	0.6667	0.5443	1
Numerical Value	7×10^{-9}	4.57	427	0.97	8.99×10^{-3}	0.664	0.5441	1.15

[a] $\Omega_{\mathrm{spher}} \equiv (M/R_p^3)^{1/2}$

[b] $I_{\mathrm{spher}} \equiv \frac{2}{3} 0.1130 \, R_p^2 M$
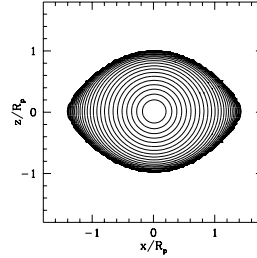
FIG. 1.— Contours of constant mass energy density $\bar{\rho}$ in a plane containing the axis of rotation for a $n = 3$ polytrope at the critical point A (see Figs. 1 and 2). Each contour marks a change of the density by a factor of $10^{1/3}$.
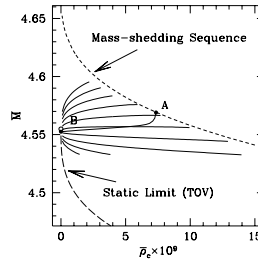

FIG. 2.— Mass versus central density plot for relativistic, rotating $n = 3$ polytropes. The long dashed curve is the TOV solution for non-rotating, static configurations, and the short dashed curve marks the mass-shedding limit. The thin solid lines denote sequences of constant angular momentum, ranging from $\bar{J} = 15$ (lowest curve) to $\bar{J} = 24$ (highest curve) in increments of $\Delta\bar{J} = 1$. Turning points of these curves mark the onset of instability. The thick solid line connects these turning points (see also Figure 3) and hence separates a region of stable configurations (above this line) from a region of unstable configurations (below this line). In particular, all nonrotating $n = 3$ polytropes are unstable to radial perturbations. A configuration evolving along the mass-shedding sequence with increasing central density becomes unstable at the critical point A. All sequences of constant angular momentum connect the mass-shedding limit with point B for $\rho_c \to 0$ (and hence $R \to \infty$). The mass of this configuration should agree with the mass $\bar{M} = 4.5525$ of a Newtonian $n = 3$ polytrope (equation (26)), which we have marked by the open circle. The deviation of the solid point B from the analytical value is a measure of our numerical accuracy.
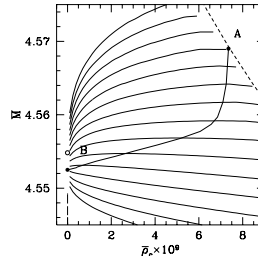

FIG. 3.— Blowup of Figure 2. Here, the thin solid lines denote sequences of constant angular momentum raging from $\bar{J} = 17.5$ (lowest curve) to $\bar{J} = 21$ (highest curve) in increments of $\Delta\bar{J} = 0.25$.

stabilized by rotation until it reaches point A. At this point, the star becomes unstable to radial perturbations and will collapse. We summarize the numerical parameters characterizing point A in Table 2, where they are compared with the findings of the analytical model calculation of Section 3.2. Figure 1 shows the density profile at the critical point A in a plane containing the axis of rotation.

Note that the numerical accuracy of an individual stellar model is fairly high. From the agreement of the limiting value B (solid dot in Figures 2 and 3) with the theoretical value (open circle), we estimate the numerical errors to be much less than 1 %. Identifying the critical point A, however, requires locating the turning points along fairly flat curves, which therefore introduces a larger error. Nevertheless, we expect that we can identify the characteristical parameters of point A to, typically, within less than 5%. Some of these parameters, however, change only very little along the mass-shedding sequence and can therefore by determined to much higher accuracy (for example $T/|W|$). The number of digits in Table 2 reflects the uncertainty in each parameter.

Having constructed self-consistent models of rotating $n = 3$ polytropes, we can now evaluate the quality of the predictions of the Roche approximation (see Section 3.1). We find that the predictions concerning the envelope alone, namely the ratio between equatorial and polar radius and the orbital frequency at mass shedding, are very accurate (Table 2). Figure 1 also shows that, at mass-shedding, only the envelope is distorted, while the core of the star remains nearly spherical. To predict $T/|W|$ at mass-shedding, the Roche approximation assumes the moment of inertia as well as the potential energy of the distorted star to be that of the corresponding spherical star, which yields $T/|W| = 0.00744$, independent of $\bar{\rho}_c$. In reality, the moment of inertia will be larger for the rotating star (by about 15% for configuration A, see the last column in Table 2), and the magnitude of the potential energy slightly smaller. Accordingly, we find that the Roche approximation underestimates $T/|W|$ by about 20%. We also find that $T/|W|$ is not independent of $\bar{\rho}_c$ (see Figure 4). However, over our region of interest, $T/|W|$ changes by much less than 1%, so that it can very well be approximated by[2] $T/|W| = 0.009$ (cf. Table 1 in Hachisu 1986).

3.4. Numerical Values in cgs units

To obtain numerical values in cgs units from the dimensionless "barred" quantities, we have to restore the polytropic constant K as well as c and G. Using eq. (5) for K, we find for the density ρ

$$\rho_c = K^{-3}\bar{\rho}_c \qquad (39)$$

$$= 9 \times 10^{10}\,\mathrm{g\,cm^{-3}} \left(\frac{M}{M_\odot}\right)^{-2} \left(\frac{\bar{\rho}_c}{7.0 \times 10^{-9}}\right),$$

where 7.0×10^{-9} is the approximate value of the central density of the critical configuration A. The temperature can now be found, for example, from eq. (17.2.9) in Shapiro

& Teukolsky (1983)

$$T_c = 9 \times 10^{10}\mathrm{K} \left(\frac{M}{M_\odot}\right)^{-1/2} \left(\frac{\bar{\rho}_c}{7.0 \times 10^{-9}}\right)^{1/3}. \qquad (40)$$

For SMSs with masses $M \gtrsim 10^6 M_\odot$, the central temperature is always less than $6 \times 10^7 K$. According to Fowler (1966), this is the minimum temperature required for generating the SMS's luminosity via the CNO cycle. This justifies our assumption that nuclear reactions can be neglected.

4. QUASISTATIONARY EVOLUTION TO THE ONSET OF INSTABILITY

In this Section we discuss the evolution of a rotating SMS up to the onset of instability. In particular, we derive analytic expressions for the evolution of the mass, radius and angular momentum as a function of time.

The evolution of the three quantities is not independent. Instead, they are coupled by two relations, namely the requirement that the star evolves along mass-shedding (so that $T/|W|$ remains approximately constant), and that the angular momentum loss can be computed from the mass that leaves that star from the equator with the critical angular velocity. This means that we can express, for instance, the angular momentum loss $\dot{J}$ and the change of radius $\dot{R}$ in terms of the mass loss $\dot{M}$. The only relation that is yet to be determined fixes $\dot{M}$ and hence the overall timescale for the evolution of the three quantities.

In a similar calculation, Bisnovatyi-Kogan, Zel'dovich & Novikov (1967) estimated $\dot{M}$ by constructing an approximate stellar wind model, which they joined onto the outer envelope of the star. Their model depends on several unknown nondimensional parameters dealing with the wind solution. Here, we take a much more naive approach, determining the mass loss rate from the requirement that the star remain in equilibrium as it cools in a quasistationary manner. According to eq. (4), the mass loss rate is related to the change of K (or the entropy), and is thus governed by the star's luminosity (see eq. (45) below).

As we have seen in Section 3.2, the post-Newtonian corrections and rotational contributions to the energy functional (20) are important for determining the stability of SMSs, but they have a very small effect on the equilibrium structure and can therefore be neglected for the purposes of this Section. Accordingly, the mass M of the star is well approximated by the Newtonian expression (4), which only depends on the polytropic constant K. The time derivative of the mass is given by

$$\frac{\dot{M}}{M} = \frac{3}{2}\frac{\dot{K}}{K}. \qquad (41)$$

The change of the total entropy S of the star is related the luminosity by

$$L = -T\dot{S}. \qquad (42)$$

Using the first law of thermodynamics, the right hand side can be rewritten

$$T\dot{S} = \int (T\dot{s})dm = \dot{K}\int n\rho^{1/n}dm = U\frac{\dot{K}}{K}, \qquad (43)$$

---

[2] Note that the relativistic definitions used to calculate T and W numerically are given in Cook, Shapiro & Teukolsky (1992), eq. (56) and (65)
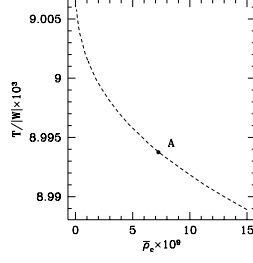
Fig. 4.— $T/|W|$ as a function of central density along the mass-shedding line. The dot marks the critical configuration A (see Figs. 2 and 3). The numerical calculation yields a value of $T/|W|$ which is different from the value $(T/|W|)_{\rm shedd} = 0.00744$ that the Roche approximation predicts. Note, however, that $T/|W|$ changes by far less than a percent over the region of interest, and can therefore well be approximated to be constant.

where U is the internal energy (see Baumgarte & Shapiro 1998, eq. [A38]). For $n = 3$ polytropes in equilibrium, the internal energy is equal to the negative of the gravitational potential energy

$$U = -W = \frac{3}{2}\frac{M^2}{R} \tag{44}$$

(see eq. (21), when post-Newtonian and rotational corrections are neglected). Collecting terms, we now find

$$\frac{\dot{M}}{M} = -\frac{L}{M}\frac{R}{M}. \tag{45}$$

The luminosity L can be written as

$$L = \lambda L_{\rm Edd}, \tag{46}$$

where the Eddington luminosity $L_{\rm Edd}$ has been defined in (7). As we have shown in Paper I, the luminosity of a SMS, rotating at the mass-shedding limit, is reduced by about 36%

$$\lambda_{\rm shedd} = 0.639. \tag{47}$$

Inserting (46) into (45), we now find

$$\frac{\dot{M}}{M} = -\frac{4\pi\lambda}{\kappa}\frac{R}{M}. \tag{48}$$

As we have seen in Section 3, a SMS that evolves along the mass-shedding limit conserves $T/|W|$ to very good approximation:

$$\frac{T}{|W|} \sim const. \tag{49}$$

Since $T/|W|$ is proportional to $J^2 M^{-3} R^{-1}$, this implies

$$\frac{\dot{R}}{R} = 2\frac{\dot{J}}{J} - 3\frac{\dot{M}}{M}. \tag{50}$$

Assuming that the mass-shedding occurs at the equator, we can write

$$\dot{J} = l_{\rm esc}\dot{M}, \tag{51}$$

where $l_{\rm esc}$ is the specific angular momentum of the escaping matter

$$l_{\rm esc} = \Omega_{\rm shedd}R_e^2 = \frac{9}{4}\Omega_{\rm shedd}R_p^2. \tag{52}$$

Since J can be written

$$J = I\Omega_{\rm shedd} = \frac{2}{3}\langle r^2\rangle M\Omega_{\rm shedd}$$
$$= \frac{2}{3}0.1130\,R_p^2 M\Omega_{\rm shedd}, \tag{53}$$

we find

$$\frac{\dot{J}}{J} = \left(\frac{3}{2}\right)^3\frac{1}{0.1130}\frac{\dot{M}}{M}. \tag{54}$$

Inserting this into (50) yields

$$\frac{\dot{R}}{R} = 3\frac{\dot{M}}{M}\left(\left(\frac{3}{2}\right)^2\frac{1}{0.1130} - 1\right). \tag{55}$$

Eqs. (48), (54) and (55) now completely determine the evolution of M, J and R. The equations can be simplified by defining the coefficients

$$k_M \equiv 4\pi\lambda_{\rm shedd} = 8.03$$
$$k_J \equiv \left(\frac{3}{2}\right)^3\frac{1}{0.1130} = 29.86, \tag{56}$$
$$k_R \equiv 2k_J - 3 = 56.73,$$

in terms of which eqs. (48), (54) and (55) can then be rewritten

$$\frac{\dot{M}}{M} = -\frac{k_M}{\kappa}\frac{R}{M} \tag{57}$$

$$\frac{\dot{R}}{R} = k_R\frac{\dot{M}}{M} \tag{58}$$

$$\frac{\dot{J}}{J} = k_J\frac{\dot{M}}{M}. \tag{59}$$

The last two equations can be integrated immediately

$$\frac{R}{R_{\rm crit}} = \left(\frac{M}{M_{\rm crit}}\right)^{k_R} \tag{60}$$

$$\frac{J}{J_{\rm crit}} = \left(\frac{M}{M_{\rm crit}}\right)^{k_J} \tag{61}$$

Inserting (60) into (57) then yields

$$\dot{M} = -\frac{k_M R_{\rm crit}}{\kappa}\left(\frac{M}{M_{\rm crit}}\right)^{k_R} \tag{62}$$

or

$$\int_{M_{\rm crit}}^{M} M^{-k_R}dM = -\frac{k_M}{\kappa}\frac{R_{\rm crit}}{M_{\rm crit}^{k_R}}\int_0^t dt, \tag{63}$$

which can be integrated to

$$\frac{M}{M_{\mathrm{crit}}} = \left(1 + \frac{(k_R - 1)k_M}{\kappa}\left(\frac{R}{M}\right)_{\mathrm{crit}} t\right)^{1/(1-k_R)}, \quad (64)$$

where $-\infty \leq t \leq 0$ and $t = 0$ corresponds to arrival at the critical configuration. Defining

$$t_{\mathrm{crit}} \equiv \frac{\kappa}{(k_R - 1)\, k_M}\left(\frac{M}{R}\right)_{\mathrm{crit}}, \quad (65)$$

the last equation can be rewritten

$$\frac{M}{M_{\mathrm{crit}}} = \left(1 + \frac{t}{t_{\mathrm{crit}}}\right)^{1/(1-k_R)} \quad (66)$$

Note that t_{crit} is independent of the mass of the star, and determines the evolutionary timescale of SMSs. In cgs units, it takes the value

$$t_{\mathrm{crit}} = \frac{c}{G}\frac{\kappa}{(k_R - 1)\, k_M}\left(\frac{GM}{c^2 R}\right)_{\mathrm{crit}} = 8.8 \times 10^{11}\mathrm{s} \quad (67)$$

(compare Shapiro & Teukolsky 1983, where a similar timescale has been derived for SMSs that are stabilized by gas pressure rather than rotation).

Similar expressions for R and J can be found by inserting (66) into (60) and (61):

$$\frac{R}{R_{\mathrm{crit}}} = \left(1 + \frac{t}{t_{\mathrm{crit}}}\right)^{k_R/(1-k_R)} \quad (68)$$

$$\frac{J}{J_{\mathrm{crit}}} = \left(1 + \frac{t}{t_{\mathrm{crit}}}\right)^{k_J/(1-k_R)} \quad (69)$$

Using the identity $k_R = 2k_J - 3$, we find that the dimensionless quantities J/M^2 and R/M evolve according to

$$\frac{J/M^2}{(J/M^2)_{\mathrm{crit}}} = \left(1 + \frac{t}{t_{\mathrm{crit}}}\right)^{-1/2} \quad (70)$$

$$\frac{R/M}{(R/M)_{\mathrm{crit}}} = \left(1 + \frac{t}{t_{\mathrm{crit}}}\right)^{-1} \quad (71)$$

We plot M, J/M^2 and R/M as a function of time in Figure 5. Note that J/M^2 and R/M evolve on the timescale t_{crit}, which is why we adopt this value for our estimates in Section 2. The mass M and similarly K, however, effectively evolve on a much longer timescale, which is a consequence of the small numerical value of the exponent $1/(1 - k_R) = -0.0179$.

5. THE OUTCOME OF COLLAPSE: SPECULATIONS

Once the supermassive star becomes unstable, it will start to collapse on a dynamical timescale. The outcome of this collapse depends on many factors, and can be determined only with a numerical, three-dimensional hydrodynamics simulation in general relativity. Such a calculation is only now underway (Baumgarte, Shapiro & Shibata 1999). The only dynamical, fully relativistic simulations

of the collapse of SMSs have been performed for nonrotating configurations in spherical symmetry (see, for example, Shapiro & Teukolsky, 1979), for which black hole formation is well established. These calculations, however, do not shed much light on the problem at hand, since rotation may play a crucial role in the dynamical evolution. The issue of the final fate of a collapsing, rapidly rotating SMS can therefore only be resolved by nonspherical, relativistic numerical simulations.

In the meantime, however, we can attempt to assess crudely whether this collapse can actually lead to the formation of a supermassive black hole. To do so, we assume that each mass shell conserves its angular momentum during the collapse (cf. the discussion at the end of Section 2), and consider two criteria.

First, a particle can only be captured by a black hole if it is not be repelled by the angular momentum barrier. For simplicity, we take the newly formed black hole to be a Schwarzschild black hole, in which case a particle is in a capture orbit if

$$l \leq 4m, \quad (72)$$

where l is the particle's specific angular momentum, and m the mass of the black hole. Here we ignore the effects of pressure, assuming that in relativistic collapse the matter approaches the nascent black hole supersonically by the time it enters the strong field domain.

Second, for any portion of the star to form a Kerr black hole, the angular momentum J of that portion cannot be larger than the square of its mass m

$$J/m^2 \leq 1. \quad (73)$$

We crudely evaluate these two criteria neglecting post-Newtonian corrections and nonspherical distortions due to rotation[3].

The specific angular momentum of a particle at radius r in the equatorial plane, at the onset of instability, is

$$l = r^2 \Omega_{\mathrm{shedd}}, \quad (74)$$

where the critical orbital velocity Ω_{crit} can be written

$$\Omega_{\mathrm{shedd}} = \left(\frac{2}{3}\right)^{3/2}\left(\frac{M}{R^3}\right)^{1/2} = \left(\frac{2}{3}\right)^{3/2}\left(\frac{R}{M}\right)_{\mathrm{crit}}^{1/2}\frac{M}{R^2}. \quad (75)$$

Here, $(R/M)_{\mathrm{crit}} \sim 450$ is the uniquely determined value at the onset of instability (see Table 2). Inserting the last two equations into (72), we find

$$\frac{m(r)}{r^2} \geq \frac{1}{4}\left(\frac{2}{3}\right)^{3/2}\left(\frac{R}{M}\right)_{\mathrm{crit}}^{1/2}\frac{M}{R^2}, \quad (76)$$

where we have assumed that the mass of the black hole, m, is the mass enclosed by a sphere of radius r.

It is convenient to express the density and radius in terms of the dimensionless Lane-Emden functions θ and ξ

$$\begin{aligned} \rho &= \rho_c\, \theta^n \\ r &= a\, \xi, \end{aligned} \quad (77)$$

where a has units of length and is defined by

$$a = \left(\frac{(n+1)K\rho_c^{(1-n)/n}}{4\pi}\right)^{1/2} \quad (78)$$

[3]In reality, interior distortions and angular momentum exchange may play an important role late in the collapse, in particular if bars form, as we argue below.
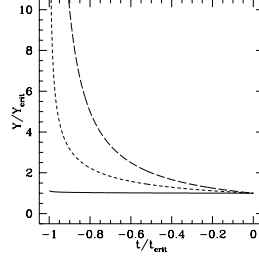
FIG. 5.— Evolutionary tracks of the mass M (solid line), angular momentum J/M^2 (short dashed line) and radius R/M (long dashed line), all normalized to their critical values at the onset of radial collapse (configuration A). The critical time $t_{\rm crit}$ is defined in eq. (65), and $t = 0$ corresponds to the time at which the star reaches this onset of instability.
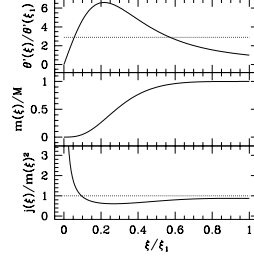

FIG. 6.— Plots of the derivative of the Lane-Emden function $\theta(\xi)$, the enclosed mass $m(\xi)$ and the enclosed angular momentum $J(\xi)$ divided by $m(\xi)^2$ as a function of ξ for $n = 3$. The horizontal, dotted line in the top panel marks the threshold for capture by a central black hole, and the dotted line in the bottom panel marks the maximum angular momentum parameter for a Kerr black hole.

(see, e.g., Shapiro & Teukolsky 1983). In terms of these quantities, the mass $m(r)$ can be written

$$m(r) = 4\pi a^3 \rho_c \xi^2 |\theta'(\xi)|, \qquad (79)$$

where the prime denotes a derivative with respect to ξ. For $n = 3$, the values of ξ and θ' at the surface of the star are $\xi_1 = 6.897$ and $|\theta'(\xi_1)| = 0.0424$. Using (77) and (79), we find that (76) reduces to a criterion on $\theta'(\xi)$ alone:

$$\frac{\theta'(\xi)}{\theta'(\xi_1)} \geq \frac{1}{4}\left(\frac{2}{3}\right)^{3/2}\left(\frac{R}{M}\right)_{\rm crit}^{1/2} \sim 2.887, \qquad (80)$$

where we have adopted $(R/M)_{\rm crit} \sim 450$ for the critical configuration.

We plot $\theta'(\xi)/\theta'(\xi_1)$ as a function of ξ in the top panel of Figure 6, and mark the threshold value 2.887 by the horizontal line. A particle at a radius for which $\theta'(\xi)/\theta'(\xi_1)$ is greater than this value can be captured, if the regions interior to this radius have collapsed to a black hole. For $\xi > \xi_{\rm max} \sim 0.57\,\xi_1$, $\theta'(\xi)/\theta'(\xi_1)$ is less than the capture threshold, and therefore the angular momentum barrier would prevent these regions from being caught by a newly formed, interior black hole. For the outermost regions, this is not surprising, since the configuration is critically rotating. Therefore, the outer region may remain in orbit, perhaps in a circumstellar disk, even if the rest of the star has collapsed. However, from the middle panel in Figure 6 we find that this outer region only contains 5% of the mass, while about 95% of the mass could form a black hole. This, again, is a consequence of $n = 3$ polytropes being extremely centrally condensed.

According to Figure 6, the angular momentum barrier would also prevent particles at very small radii, $\xi \lesssim 0.05\xi_1$, from being captured by a black hole interior to that radius. However, for this to be relevant, the initial black hole would have to be restricted to a very small fractional

size, and as we will see below, the second criterion (73) does not allow such small black holes to form.

We may reverse the above argument and view eq. (80) as a condition on R/M. Since the left hand side, $\theta'(\xi)/\theta'(\xi_1)$, has a maximum of about 6.6, R/M has to be smaller than about 2350 for black hole formation to be possible. It is interesting that R/M of the critical configuration A is only about five times smaller than this threshold compaction, just barely allowing the supermassive star to form a supermassive black hole. This argument suggests that primordial gas may have to pass through a phase as a SMS where it can lose angular momentum before it can possibly collapse to a SMBH.

We can similarly evaluate the second criterion, eq. (73), in terms of Lane-Emden functions. The angular momentum $J(r)$ of the matter enclosed within radius r, rotating with the critical angular velocity, can be written

$$
\begin{aligned}
J(r) &= I(r)\,\Omega_{\rm shedd} \\
&= \left(\frac{2}{3}\right)^{3/2}\left(\frac{R}{M}\right)_{\rm crit}^{1/2}\frac{M}{R^2}\frac{8\pi}{3}\int_0^r \rho r^4 dr \qquad (81) \\
&= \left(\frac{2}{3}\right)^{5/2}\left(\frac{R}{M}\right)_{\rm crit}^{1/2}(4\pi)^2 a^6 \rho_c^2 |\theta'(\xi_1)|\int_0^\xi \theta^n \xi^4 d\xi.
\end{aligned}
$$

Dividing this by the square of the mass, eq. (79), then yields the condition

$$1 \geq \frac{J(\xi)}{m(\xi)^2} = \left(\frac{2}{3}\right)^{5/2}\left(\frac{R}{M}\right)_{\rm crit}^{1/2}\frac{|\theta'(\xi_1)|}{\xi^4|\theta'(\xi)|^2}\int_0^\xi \theta^n \xi^4 d\xi. \quad (82)$$

In the bottom panel of Figure 6 we show the right hand side of this equation for a $n = 3$ polytrope and for $(R/M)_{\rm crit} = 450$. The dotted, horizontal line is the critical value of unity. A region inside a radius ξ can form a

Kerr black hole only if $J(\xi)/m(\xi)^2$ is less than unity. This condition is satisfied everywhere except for the innermost regions $\xi < \xi_{\min} \sim 0.1 \xi_1$. At the surface, $\xi = \xi_1$, we recover the value $(J/M)^2_{\text{crit}} = 0.876$ found in eq. (33).

Note that for any polytrope, m is proportional to r^3 for small radii r and J is proportional to $m(r)\Omega r^2 \sim \Omega r^5$. Therefore, J/m^2 scales like Ω/r close to the center, which prevents the formation of arbitrarily small black holes from rotating polytropes. In our case, the region inside $\xi_{\min} \sim 0.1 \xi_1$, containing about 4% of the total mass, defines the minimum mass which can collapse to form an initial black hole. Since $\theta'(\xi)/\theta'(\xi_1)$ exceeds the threshold for $\xi \gtrsim \xi_{\min}$, such a "minimal" seed black hole could accrete further material from the star.

Finally, we note that a bar instability may form during the collapse of the star. The criterion for the formation of a bar on a dynamical timescale is

$$\left(\frac{T}{|W|}\right)_{\text{bar}} \gtrsim 0.27 \qquad (83)$$

(see, e.g., Chandrasekhar 1969; Shapiro & Teukolsky 1983). Since M and J are approximately conserved during the collapse, $T/|W|$ scales with R^{-1}, so a bar will start to form when

$$\frac{R_{\text{bar}}}{R_{\text{crit}}} = \left(\frac{T}{|W|}\right)_{\text{crit}} \left(\frac{T}{|W|}\right)_{\text{bar}}^{-1} \sim \frac{0.009}{0.27} = \frac{1}{30}. \qquad (84)$$

The value of R/M at bar formation is then

$$\left(\frac{R}{M}\right)_{\text{bar}} \sim \frac{1}{30}\left(\frac{R}{M}\right)_{\text{crit}} \sim 15. \qquad (85)$$

Eg. (85) suggests that the collapsing star may form a non-axisymmetric bar before it forms a black hole. This is an important result, since such a bar may result in a quasiperiodic emission of gravitational waves (cf. Smith, Houser & Centrella 1996). The frequency of these waves can be estimated from the expected bar rotation rate

$$f_{\text{bar}} \sim \frac{\Omega_{\text{bar}}}{2\pi} \sim \frac{1}{2\pi}\left(\frac{M}{R_{\text{bar}}^3}\right)^{1/2} = \frac{1}{2\pi}\left(\frac{M}{R_{\text{bar}}}\right)^{3/2}\frac{1}{M}$$

$$\sim 5 \times 10^2 \,\text{Hz} \left(\frac{M}{M_\odot}\right)^{-1}. \qquad (86)$$

For a SMS of $10^6 M_\odot$ this yields a frequency of 5×10^{-4} Hz, which is in the range in which LISA is expected to be most sensitive (see, e.g., Thorne 1995). The frequency increases at later stages of the collapse, when M/R_{bar} becomes larger. The strength of the gravitational wave signal can be crudely estimated to be

$$h \sim \frac{\ddot{Q}}{d} \sim \frac{MR_{\text{bar}}^2 f_{\text{bar}}^2}{d} \sim \frac{M}{d}\frac{1}{4\pi^2}\frac{M}{R_{\text{bar}}}$$

$$\sim 10^{-25}\left(\frac{M}{M_\odot}\right)\left(\frac{d}{1\text{Gpc}}\right)^{-1}, \qquad (87)$$

where Q is the star's quadrupole moment, and d is the distance, which we scale to 1 Gpc (the Hubble distance is ~ 3 Gpc). The signal strength increases with M/R_{bar} at late stages of the collapse. Apart from any bar, the implosion itself will be nonspherical, due to rotation, and will result

in a gravitational wave burst. The collapse of a supermassive star may therefore be a very promising candidate for detection by space based gravitational wave detectors (LISA Pre-Phase A report 1995).

Obviously, the arguments presented in this section are very crude and do not replace a fully self-consistent relativistic hydrodynamical calculation. Our arguments nevertheless suggest that, upon reaching the onset of instability, supermassive stars may form a supermassive black hole, containing a large part of the mass, and leaving only a few percent of the initial mass outside of the black hole, most likely in the form of a disk. We furthermore anticipate that a bar may form during the collapse, which may lead to the emission of quasiperiodic gravitational waves.

6. SUMMARY

We have launched a fully relativistic study of the formation of SMBHs via the collapse of SMSs. In this paper we study the quasistationary, secular evolution of SMSs up to the critical configuration at which radial instability sets in and focus on the effects of rotation and general relativity. We identify the critical configuration and its characteristic parameters R/M, $T/|W|$ and J/M^2. These parameters are independent of the mass of the SMS, and are therefore universal constants. The subsequent implosion, starting from this universal critical configuration, is therefore also uniquely determined and should produce a unique gravitational waveform. We compare results from an analytic, approximate treatment and a fully relativistic, numerical calculation, and find good agreement. We furthermore solve analytically for the time evolution of these parameters up to the onset of instability.

Identifying the critical configuration at the onset of instability is interesting for its own sake. More importantly, however, this configuration will be adopted as initial data for future numerical simulations of SMS collapse (Baumgarte, Shapiro & Shibata 1999). In this paper we assemble qualitative arguments to anticipate the outcome of the collapse and find that the formation of a SMBH containing an appreciable fraction of the mass is not ruled out. Our arguments suggest that a transient phase as a SMS may be an efficient way for primordial gas to lose sufficient angular momentum in order to overcome the Kerr angular momentum barrier to forming a SMBH.

Loeb & Rasio (1994) have emphasized that SMBHs appear to have a minimum "observed" mass of $\sim 10^6 M_\odot$. Our crude arguments may help to explain this minimum in the context of the SMS formation scenario. SMSs with masses less than this value will not evolve in a quasistationary manner up to our critical configuration A, because some of our assumptions break down. For example, nuclear burning may cause the star to explode (Appenzeller & Fricke 1972, Fuller, Woosley & Weaver, 1986). Electron-positron pairs may also be important for small masses, and may destabilize the star (see Zel'dovich & Novikov 1971) before it reaches a small enough value of R/M to overcome the angular momentum barrier. On the other hand, all SMSs with $M \gtrsim 10^6 M_\odot$ will evolve in a quasistationary manner until reaching the critical configuration A. The subsequent collapse will likely give rise to a SMBH of almost the same mass as the progenitor SMS.

REFERENCES

Appenzeller, I., & Fricke, K. J., 1972, A&A, 21, 285
Balbus, S. A., & Hawley, J. F., 1991, ApJ, 376, 214
Baumgarte, T. W., & Shapiro, S. L., 1998, ApJ, 504, 431
—, 1999, submitted (paper I)
Baumgarte, T. W., Shapiro, S. L., & Shibata, M., 1999, in preparation
Begelman, M. C., & Rees, M., J., MNRAS, 185, 847
Bisnovatyi-Kogan, G. S., 1998, ApJ, 497, 559
Bisnovatyi-Kogan, G. S., Zel'dovich, Ya. B., & Novikov, I. D., 1967, Soviet Astron., 11, 419
Chandrasekhar, S., 1964a, Phys. Rev. Lett., 12, 114, 437E
Chandrasekhar, S., 1964b, ApJ, 140, 417
Chandrasekhar, S., 1969, Ellipsoidal Figures of Equilibrium (Yale University Press, New Haven)
Claussen, M. J., & Lo, K. Y., 1986, ApJ, 308, 592
Cook, G. B., Shapiro, S. L., & Teukolsky, S. A, 1992, ApJ, 398, 203
—, 1994, ApJ, 422, 227
Fowler, W. A., 1964, Rev. Mod. Phys., 36, 545, 1104E
—, 1966, ApJ, 144, 180
Friedman, J. L., Ipser, R. R., & Sorkin, R. D., ApJ, 325, 722
Fuller, G. M., Woosley, S. E., & Weaver, T. A., ApJ, 307, 1986
Hachisu, I., 1986, ApJS, 61, 479
Hoyle, F., and Fowler, W. A., 1963a, MNRAS, 125, 169
—, 1963b, Nature, 197, 533
Iben, I., 1963, ApJ, 138, 1090
Kippenhahn, R., and Weigert, A., 1990, Stellar Structure and Evolution (Springer)
Lai, D., Rasio, F. A., & Shapiro, S. L., 1993, ApJS, 88, 205
LISA Science Team, Laser Interferometer Space Antenna for the detection and observation of gravitational waves: Pre-Phase A Report, Dec., 1995 (also: Max-Planck Institut für Quantenoptik, Report MPQ 208, Garching, Germany, February, 1996).

Loeb, A., and Rasio, F. A., 1994, ApJ, 432, 52
Lombardi, J. C., Jr., 1997, private communication
Miyoshi, M., et. al., 1995, Nature, 373, 127
Papaloizou, J. C. B., & Whelan, F. A. J., 1973, MNRAS, 164, 1
Rees, M. J., 1984, ARA&A, 22, 471
Rees, M. J., 1998, in Black Holes and Relativistic Stars, ed. R. M. Wald (University of Chicago Press, Chicago)
Quinlan, G. D., & Shapiro, S. L., 1987, ApJ, 321, 199
—, 1990, ApJ, 356, 483
Sanders, R. H., 1970, ApJ, 162, 791
Shakura, N. I., & Sunyaev, R. A., 1973, A&A, 24, 337
Shapiro, S. L., & Teukolsky, S. A., 1979, ApJ, 234, L177
—, S. A., 1985a, ApJ, 292, L91
—, S. A., 1985b, ApJ, 298, 34
—, S. A., 1983, Black Holes, White Dwarfs, and Neutron Stars (Wiley, New York)
Smith, S. C., Houser, J. L., & Centrella, J. M., ApJ, 458, 236, 1996
Thorne, K. S., 1995, in Seventeenth Texas Symposium on Relativistic Astrophysics and Cosmology, ed. H. Böhringer, G. E. Morfill and J. E. Trümper (Annals of the New York Academy of Sciences, 759)
Thorne, K. S., & Braginsky, V. B., 1976, ApJ, 204, L1
Wagoner, R. V., 1969, ARA&A, 7, 553
Watson, W. D., & Wallin, B. K., 1994, ApJ, 432, L35
Zel'dovich, Ya. B., & Novikov, I. D., 1971 Relativistic Astrophysics, Vol. 1 (University of Chicago Press)
Zel'dovich, Ya. B., & Podurets, M. A., 1965, Astr. Zh., 42, 963 (English transl., Soviet Astr.-A. J., 9, 742 [1965])